npj | precision oncology

Article

Published in partnership with The Hormel Institute, University of Minnesota

https://doi.org/10.1038/s41698-025-00848-2

Complement activation in tumor microenvironment after neoadjuvant therapy and its impact on pancreatic cancer outcomes

Check for updates

Xiaofei Zhang[1,2,10] ✉, Ruoxin Lan[3,10], Yongjun Liu[1,4], Venu G. Pillarisetty[5], Danting Li[3], Chaohui L. Zhao[2], Suparna A. Sarkar[6], Weiguo Liu[2], Iman Hanna[2], Mala Gupta[2], Cristina Hajdu[6], Jonathan Melamed[2], Michael Shusterman[7], Jessica Widmer[8], John Allendorf[9] & Yao-Zhong Liu[3] ✉

Neoadjuvant therapy (NAT) is increasingly being used for pancreatic ductal adenocarcinoma (PDAC). This study investigates how NAT differentially impacts PDAC's carcinoma cells and the tumor microenvironment (TME). Spatial transcriptomics was used to compare gene expression profiles in carcinoma cells and the TME of 23 NAT-treated versus 13 NAT-naïve PDACs. Findings were validated by single-nucleus RNA sequencing (snRNA-seq) analysis. NAT induces apoptosis and inhibits proliferation of carcinoma cells and coordinately upregulates multiple complement genes (C1R, C1S, C3, C4B and C7) within the TME. Higher TME complement expression following NAT is associated with increased immunomodulatory and neurotrophic cancer-associated fibroblasts (CAFs); more $CD4^+$ T cells; reduced immune exhaustion gene expression, and improved overall survival. snRNA-seq analysis demonstrates C3 complement is mainly upregulated in CAFs. These findings suggest that local complement dynamics could serve as a novel biomarker for prognosis, evaluating treatment response, and guiding therapeutic strategies in NAT-treated PDAC patients.

Pancreatic ductal adenocarcinoma (PDAC) is a highly aggressive cancer with a five-year survival rate of 11%[1]. It is projected to become the second leading cause of cancer-related deaths in the United States by 2030[2]. Only 15–20% of patients are eligible for surgery, as most patients present with locally advanced unresectable disease or distant metastases[3]. Furthermore, since most patients who undergo surgical resection ultimately succumb to their disease, systemic chemotherapy is a necessary therapeutic component for most patients[4].

PDAC presents a significant therapeutic challenge due to its resistance to various treatment modalities including immune checkpoint inhibitor therapy[5–7]. It exhibits extensive genetic diversity, leading to the development of subpopulations with diverse molecular alterations and resistance mechanisms[8]. The tumor microenvironment (TME) in PDAC is highly immunosuppressive, characterized by the presence of immunosuppressive cells, cytokines, and chemokines that impede effective anti-tumor immune responses despite the presence of large numbers of effector T cells[9–11]. Additionally, the TME plays a pivotal role in influencing tumor growth and metastasis through its impact on mitochondrial biogenesis, blood supply, and nutrient availability[12]. These factors contribute to the high therapeutic resistance observed in PDAC, highlighting the need for innovative combinational strategies to improve treatment outcomes.

Neoadjuvant therapy (NAT) has emerged as the preferred approach for managing resectable and borderline resectable PDAC over adjuvant therapy for several reasons. NAT offers better tolerability for patients by

[1]Department of Pathology and Laboratory Medicine, University of Wisconsin-Madison, Madison, WI, USA. [2]Department of Pathology and Laboratory Medicine, New York University Grossman Long Island School of Medicine, Mineola, NY, USA. [3]Department of Biostatistics and Data Science, Tulane University School of Public Health and Tropical Medicine, New Orleans, LA, USA. [4]Department of Laboratory Medicine and Pathology, University of Washington School of Medicine, Seattle, WA, USA. [5]Department of Surgery, University of Washington School of Medicine, Seattle, WA, USA. [6]Department of Pathology and Laboratory Medicine, New York University Grossman School of Medicine, New York, NY, USA. [7]Department of Oncology, New York University Grossman Long Island School of Medicine, Mineola, NY, USA. [8]Department of Gastroenterology, New York University Grossman Long Island School of Medicine, Mineola, NY, USA. [9]Department of Surgery, New York University Grossman Long Island School of Medicine, Mineola, NY, USA. [10]These authors contributed equally: Xiaofei Zhang, Ruoxin Lan. ✉e-mail: xiaofei.zhang@nyulangone.org; yliu8@tulane.edu

The Hormel Institute
University of Minnesota

administering chemotherapy and/or radiation prior to surgery, taking advantage of patients' relatively better overall health status and minimizing treatment-related complications[13,14]. NAT also effectively increases tumor resectability and R0 resection rate by downstaging locally advanced disease and facilitating complete tumor removal[7,15]. Moreover, NAT may target early metastases, potentially improving treatment outcomes[7,15]. NAT also provides an opportunity to observe an individual patient's response to therapy and to select suitable candidates for surgery[7,15]. Some studies suggested that NAT may be associated with improved overall survival rates compared to adjuvant therapy[13,14]. Furthermore, recent studies suggested that NAT may have the potential to prime the stroma and enhance the response to immunotherapy in various cancers[16,17]. By modulating TME, NAT may render PDAC more susceptible to immunotherapeutic interventions[16,17].

Single-cell RNA sequencing (scRNA-seq) is a valuable tool for characterizing TME as it provides insights into cellular heterogeneity and molecular subtypes[18,19]. Several scRNA-seq studies have explored the PDAC TME, offering valuable insights into this complex ecosystem[20–36]. However, scRNA-seq techniques lack spatial context, and are susceptible to cell dissociation-associated artifacts. Spatial transcriptomic analysis complements and extends the scope of single-cell studies[37,38] by providing valuable insights into the spatial distribution of gene expression and a holistic characterization of the PDAC TME. To obtain a comprehensive view of the PDAC TME and its response to NAT, we performed a comparative spatial transcriptomic study using formalin-fixed paraffin-embedded (FFPE) specimens from PDAC patients who received NAT before surgery versus those who underwent upfront surgery without NAT.

Results

Intra- and intertumoral heterogeneity of NAT response in PDAC carcinoma and TME

The clinicopathologic characteristics of the 36 patients in our study cohort are summarized in Fig. 1A and Supplementary Table 1. This cohort includes 23 patients who had surgery after receiving neoadjuvant chemotherapy (the NAT group) and 13 age-, gender-, and stage-matched patients who had upfront surgery (the naïve group). The NAT consisted of either FOLFIRINOX or gemcitabine treatment, with or without radiation. The NAT group was further categorized into responders and non-responders based on histopathologic evaluation of tumor regression using the American Joint Committee on Cancer/College of American Pathologists Tumor Regression Grading (AJCC/CAP-TRG) system. Only resected primary PDAC specimens were used in this study except for 4 patients whose pre-NAT biopsies were included in the naïve group and post-NAT resection specimens were included in the NAT group. A separate pairwise longitudinal comparison of the pre-NAT biopsy versus the corresponding post-NAT resection specimen from the same patient was also done for these 4 patients (Fig. 1E and Supplementary Tables 2).

To assess the relative extents of intra- vs. intertumoral heterogeneity, 2 to 5 ROIs (region of interest) were selected from each subject, amounting to a total of 119 ROIs from the 36 patients in the entire cohort (Supplementary

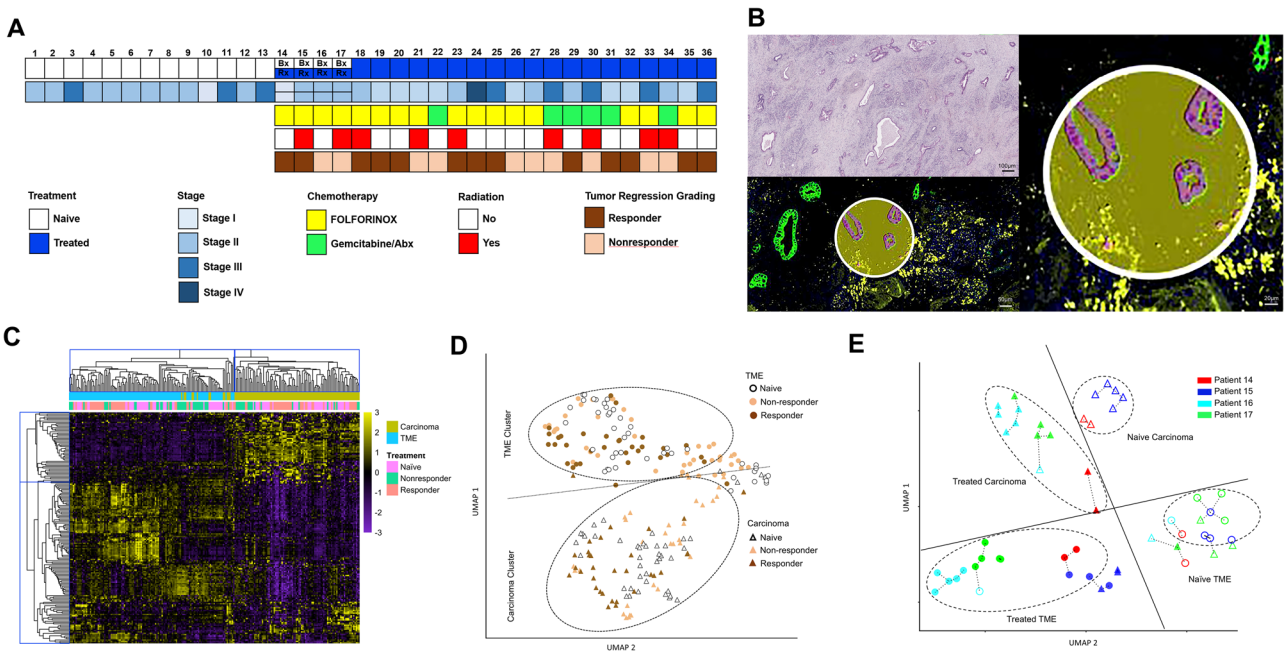


Fig. 1 | Spatial transcriptomics reveals intra- and intertumoral heterogeneity of neoadjuvant therapy (NAT) response in pancreatic ductal adenocarcinoma (PDAC) cancer cells and the tumor microenvironment (TME). A Clinical and pathologic characteristics of the 36 patients in our study cohort. For patients 14–17, both the pre-NAT biopsies (included in the naïve group) and the corresponding post-NAT resection specimen (included in the NAT group) were analyzed. For all other patients, only the respected primary PDAC specimens were used. **B** Immunofluorescence segmentation of each ROI into carcinoma AOI and TME AOI (pan-CK in green, α-SMA in yellow, DAPI in blue). Total mRNA libraries were prepared separately from each of these two AOIs for every ROI. **C** Heatmap of gene expression profiles in all 223 carcinoma and TME AOIs. Unsupervised clustering reveals a distinct separation between carcinoma AOIs and TME AOIs, with limited overlap in the middle. There is no discernible separation between the naïve group and the NAT group within either the carcinoma AOI cluster or the TME AOI cluster. Similarly, among the NAT-treated patients, there was no discernible separation between the responders and non-responders. **D** UMAP plot demonstrating near-complete separation of carcinoma AOIs and TME AOIs. A total of 95.1% (137/144) of the TME AOIs cluster above the dashed line, while 94.5% (103/109) of the carcinoma AOIs cluster below the dashed line. Approximately 5% of the AOIs overlap at the tails of these two clusters. There is no noticeable separation between the NAT group and the naïve group within either cluster. Similarly, within the NAT group, there is no noticeable separation between responders (dark brown) and non-responders (light brown) in either the carcinoma AOI cluster or the TME AOI cluster. **E**. UMAP plot of the four pairs of pre-NAT biopsy and corresponding post-NAT resection from patients 14–17 (Δ=naïve carcinoma; ▲=NAT-treated carcinoma. ○=naïve TME; ●=NAT-treated TME. Datapoints from the same patient are shown in the same color). For both carcinoma AOIs and TME AOIs, datapoints from NAT group are separated from those from the naïve group. The dotted lines connect each datapoint to its nearest neighbor. Most of the datapoints are closer to datapoints from the same patient than to those of different patients, suggesting datapoints from the same patient tend to cluster together.

Fig. 1). Using immunofluorescence staining, each ROI was segmented into two AOIs (Area of Illumination): the carcinoma AOI (pan-CK+, SMA-) containing predominantly carcinoma cells, and the TME AOI (pan-CK-, SMA+) which comprised of various types of stroma cells and immune cells (Fig. 1B). RNA libraries were prepared from these 238 AOIs, of which 223 (93.7%) passed the quality control and were used for analysis, including 42 carcinoma AOIs and 43 TME AOIs from the naïve group, and 72 carcinoma AOIs and 66 TME AOIs from the NAT group.

First, we compared the gene expression profiles of carcinoma AOIs versus TME AOIs. Carcinoma AOIs showed significantly higher expression of 302 and 321 genes than TME AOIs in the naïve group and the NAT group, respectively, with an overlap of 261 genes which included *KRT19, KRT7, KRT18, MUC1, CDH1, EPCAM, JUP, ITGA3, ITGB4, ERRB2, LAMB3, CAPN2, LGALS3, LCN2 etc*. In contrast, TME AOIs showed significantly higher expression of 286 and 294 genes than carcinoma AOIs in the naïve group and the NAT group, respectively, with an overlap of 250 genes including *PDGFRB, COL6A3, FCGR2A/B, IL1R1, etc*. (Supplementary Fig. 2, Supplementary Data 1). Hierarchical clustering analysis successfully grouped these 223 AOIs into the carcinoma cluster and the TME cluster, with a limited number of datapoints overlapped in between these two distinct clusters (Fig. 1C). There was no discernible differentiation between the naïve and NAT AOIs within either the carcinoma cluster or the TME cluster. For cases that received NAT, there was no discernible separation between the responders and the non-responders.

Next, we used a dimension reduction technique to visualize the clustering pattern of these 223 AOIs in two major UMAP dimensions based on their transcriptomics profiles. Like the results from the hierarchical clustering analysis, these 223 AOIs were largely separated into the carcinoma cluster and the TME cluster, with only a small proportion of AOIs from each category intermingling at the peripheries of these two clusters (Fig. 1D). However, notable differentiation based on treatment status (i.e., naïve vs. NAT) was once again not evident in both clusters, suggesting both carcinoma cells and the TME responded to NAT heterogeneously at the transcriptomics level. Similarly, for cases that received NAT, there was no notable segregation between the responders and the non-responders in the UMAP space.

To investigate the roles of intra- versus intertumoral heterogeneity in NAT response, we also made a UMAP plot of the four pairs of samples in which each pre-NAT biopsy was compared with its corresponding post-NAT resection specimen from the same patient. In addition to the clear separation of carcinoma from TME AOIs, a trend of separation was also noted between the naïve group (i.e., pre-NAT biopsy) and the NAT group (i.e., the post-NAT resection) in both the carcinoma cluster and the TME cluster (Fig. 1E). In accordance with the anticipated relative magnitudes of intra- versus intertumoral heterogeneity, the AOIs from the same patient tended to aggregate more closely together than those from different patients (Fig. 1E).

To compare the cellular composition within carcinoma and TME AOIs, we calculated the gene signature scores for different types of stromal cells and immune cells using our transcriptomics data. As compared to carcinoma AOIs, TME AOIs contained significantly more fibroblasts and immune cells across the board (Supplementary Fig. 3).

Effects of NAT on the carcinoma cells of PDAC

We first studied the effect of NAT on the carcinoma cells of PDAC by comparing the gene expression profiles in the carcinoma AOIs of the naïve group versus the NAT group. After controlling age, gender and other clinicopathological factors, we identified 44 NAT-induced differentially expressed genes (DEGs), including 22 upregulated and 22 downregulated (Fig. 2A, Supplementary Data 2) in the carcinoma AOIs of the NAT group. The most significantly upregulated genes include *DDB2* ($p = 7.70e-4$), *FBP1* ($p = 0.0016$) and *PRKACB* ($p = 0.0028$). The most significantly downregulated genes include *IL32* ($p = 0.0039$), *ACTB* ($p = 0.0041$) and *TPM1* ($p = 0.0059$). DAVID enrichment analysis indicated that the DEGs upregulated in the carcinoma cells by NAT were significantly enriched with functional terms related to apoptosis (KW-0053~Apoptosis, FDR = 0.013) and Ser/Thr-type protein kinases (SM00133:S_TK_X, FDR = 0.024, Fig. 2B). On the other hand, the downregulated DEGs were significantly enriched with functional terms related to chromatin (GO:0000785~chromatin, FDR = 0.0059), nucleoplasm (GO:0005654~nucleoplasm, FDR = 0.023), GO:0032991~macromolecular complex (FDR = 0.023), and KW-0488~Methylation (FDR = 0.024). These results are consistent with the expected cytoreductive effect of NAT on carcinoma cells.

Next, we investigated the impact of NAT on carcinoma cells in more detail by utilizing the recently defined gene signatures for the seven malignant cell programs representing the lineages of carcinoma cells and the seven malignant cell states[25]. Signature scores for each of these malignant programs and cell states were calculated for all carcinoma AOIs based on the geometric mean of expression levels for their respective signature genes sets. Their association with NAT was assessed after controlling age, gender, cancer size and grade. We found that there was a significant increase of acinar-like program ($p = 0.011$, Fig. 2C), a significant decrease of cycling_G2/M state ($p = 0.001$), and a marginally significant decrease of TNF-NFκB signaling ($p = 0.057$) in the NAT group. These findings were also supported by morphologic analysis, which showed increased apoptosis along with decreased proliferation and mitosis in the carcinoma cells of the NAT group compared to the naïve group (Fig. 2D).

We also compared the gene expression profiles in the carcinoma AOIs of responders versus non-responders to NAT. After controlling for age, gender and other clinicopathological factors, we identified 188 DEGs in responders when comparing to non-responders, including 72 up- and 116 downregulated genes (Fig. 2E,). The most significantly upregulated genes include *GPX4* ($p = 2.70e-4$), *TWF1* ($p = 3.90e-4$) and *FCGRT* ($p = 4.50e-4$). The most significantly downregulated genes include *CCL18* ($p = 9.10e-4$), *RAD51C* ($p = 1.10e-3$) and *CD53* ($p = 1.60e-3$). DAVID enrichment analysis of these DEGs indicated that the upregulated genes in the carcinoma cells of responders were significantly enriched with functional terms related to apoptosis (FDR = 2.17e-6) and TNF signaling pathway (FDR = 3.32e-5) (Fig. 2F). On the other hand, the downregulated genes were significantly enriched with functional terms related to cell adhesion molecules (FDR = 6.28e-5) and neutrophil chemotaxis (FDR = 1.04e-4) (Fig. 2F). In addition, compared to non-responders, the responders showed an increased squamoid program ($p = 1.22e-3$) and adhesive state ($p = 1.26e-3$), as well as a decreased cycling_G2/M state ($p = 1.56e-3$) (Fig. 2G). These findings were supported by histopathologic observations, which showed more squamoid and less high grade discohesive morphology in responders than non-responders (Fig. 2H).

Effects of NAT on the TME of PDAC

We then examined the effect of NAT on PDAC TME by comparing the gene expression profiles in the TME AOIs of the NAT group versus the naive group. After controlling age, gender, carcinoma grade and size, we identified 52 NAT-induced DEGs in the TME AOIs, including 28 upregulated and 24 downregulated (Fig. 3A, Supplementary Data 2). The top significantly upregulated genes include *CDKN1A* ($p = 3.82e-4$), *MDM2* ($p = 8.04e-4$), *FAS* ($p = 2.72e-3$) and *IL6ST* ($p = 0.0055$). The top significantly downregulated genes include *HDAC2* ($p = 2.85e-5$), *TPM1*($p = 7.21e-4$), *ACTB* ($p = 2.28e-3$) and *PKM* ($p = 0.0033$). Remarkably, there were five complement genes (*C1R, C1S, C3, C4B* and *C7*) among the significantly upregulated genes, suggesting that NAT induced a coordinated upregulation of complement pathway genes in the TME of PDAC.

DAVID enrichment analysis of these significantly upregulated DEGs showed that NAT upregulated significantly more functional terms in the TME than in the carcinoma cells of PDAC. Among those, there were three highly enriched terms related to complement pathway (Fig. 3B), including KW-0180~Complement pathway (FDR = 1.04e-5), GO:0006958~Complement activation, classical pathway (FDR = 1.06e-2), and has04610~~Complement and coagulation cascades (FDR = 1.28e-3). Additionally, there were functional terms related to immunity, including KW-0399 Innate immunity (FDR = 9.61e-3); and multiple pathways related to cancer

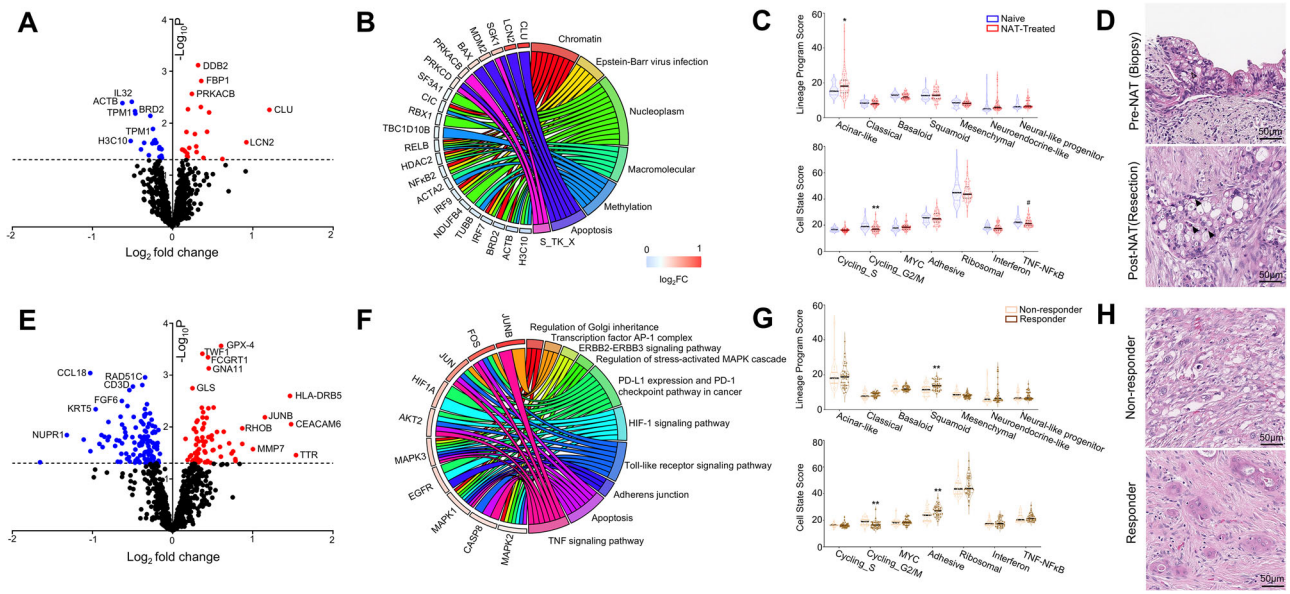


Fig. 2 | Impact of NAT on carcinoma cells in PDAC. A Volcano-plot showing differentially expressed genes (DEGs) in carcinoma cells induced by NAT. **B** Chord diagram illustrating the relationship between individual DEGs and the enriched pathways induced by NAT in carcinoma cells. **C** Impact of NAT on malignant cell lineage programs (top) and malignant cell states (bottom). NAT significantly upregulated the acinar program and downregulated the Cycling_G2/M state. TNF-NFκB signaling showed a decrease with marginal statistical significance. **D** Histologic evaluation showing that the NAT-treated carcinoma cells (bottom) exhibit significantly increased apoptosis (solid arrowhead), decreased mitosis (open arrowhead), and cytoplasmic vacuolization compared to naïve carcinoma cells (top), consistent with transcriptomics findings. **E** Volcano-plot showing DEGs in the carcinoma AOIs when comparing responders to the non-responders in the NAT group. **F** Chord diagram illustrating the relationship between individual DEGs and the enriched pathways when comparing responders versus non-responders. **G** Differences in malignant cell lineage programs (top) and malignant cell states (bottom) between responders versus non-responders in the NAT group. The squamoid lineage program and adhesive malignant state were significantly upregulated, whereas the cycling_G2/M state was significantly downregulated. **H** H&E images of a carcinoma AOI in a non-responder (top, patient#33, Cycling-G2/M score = 20.2, squamoid signature score = 25.7, adhesive state score = 19.5) versus a carcinoma AOI in a responder (lower, patient #25, Cycling-G2/M Score=14.2 squamoid signature Score=45.8, adhesive state Score=34.0). Overall, the carcinoma AOIs in the non-responder show more discohesive and less squamoid morphology with more mitoses, consistent with the transcriptomics findings. (#$p < 0.1$; *$p < 0.05$; **$p < 0.01$).

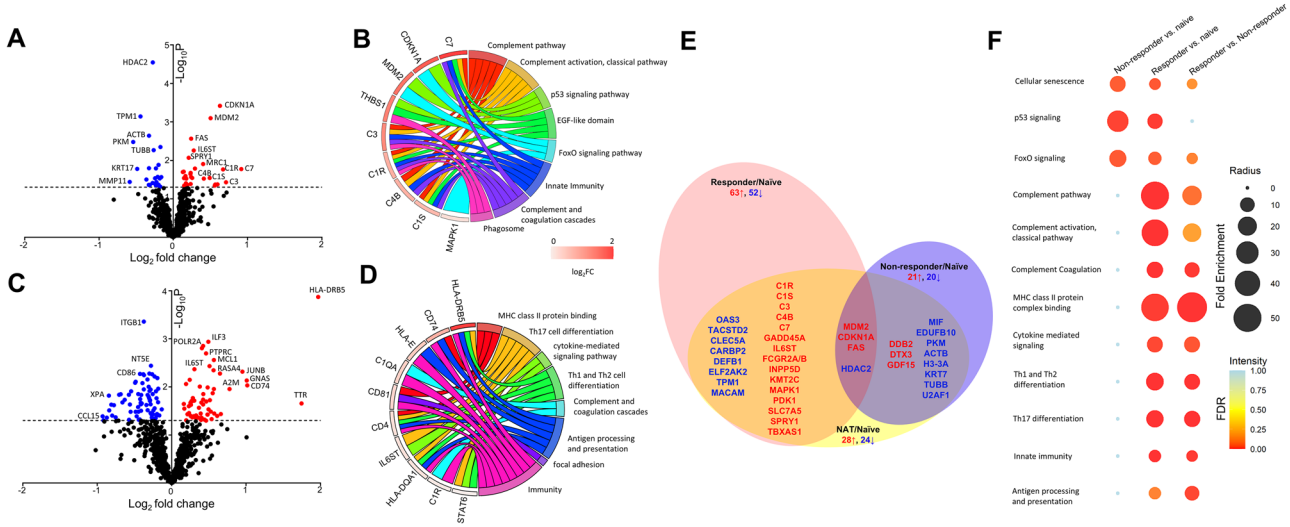


Fig. 3 | Impact of NAT on PDAC TME. A Volcano plot displaying differentially expressed genes (DEGs) in the TME of PDAC induced by NAT. **B** Chord diagram illustrating the relationship between individual DEGs and the enriched pathways. The five NAT-upregulated complement genes are broadly associated with immunomodulation pathways. **C** Volcano plot displaying DEGs in the TME when comparing responders versus non-responders of the NAT group. **D** Chord diagram illustrating the relationship between individual DEGs and the enriched pathways when comparing responders versus non-responders of the NAT group. **E** Venn diagram showing the overlap of upregulated (red font) and downregulated (blue font) genes in TME AOIs when comparing the entire NAT group (yellow), the responder subgroup (red), and the non-responder subgroup (blue) against the naïve group. Notably, the five complement genes were upregulated only in the responder subgroup. **F** Dot plot showing the most significantly enriched pathways in comparisons between responders vs. the naïve group (left), non-responders vs. the naïve group (middle), and responders vs. the non-responders (right).

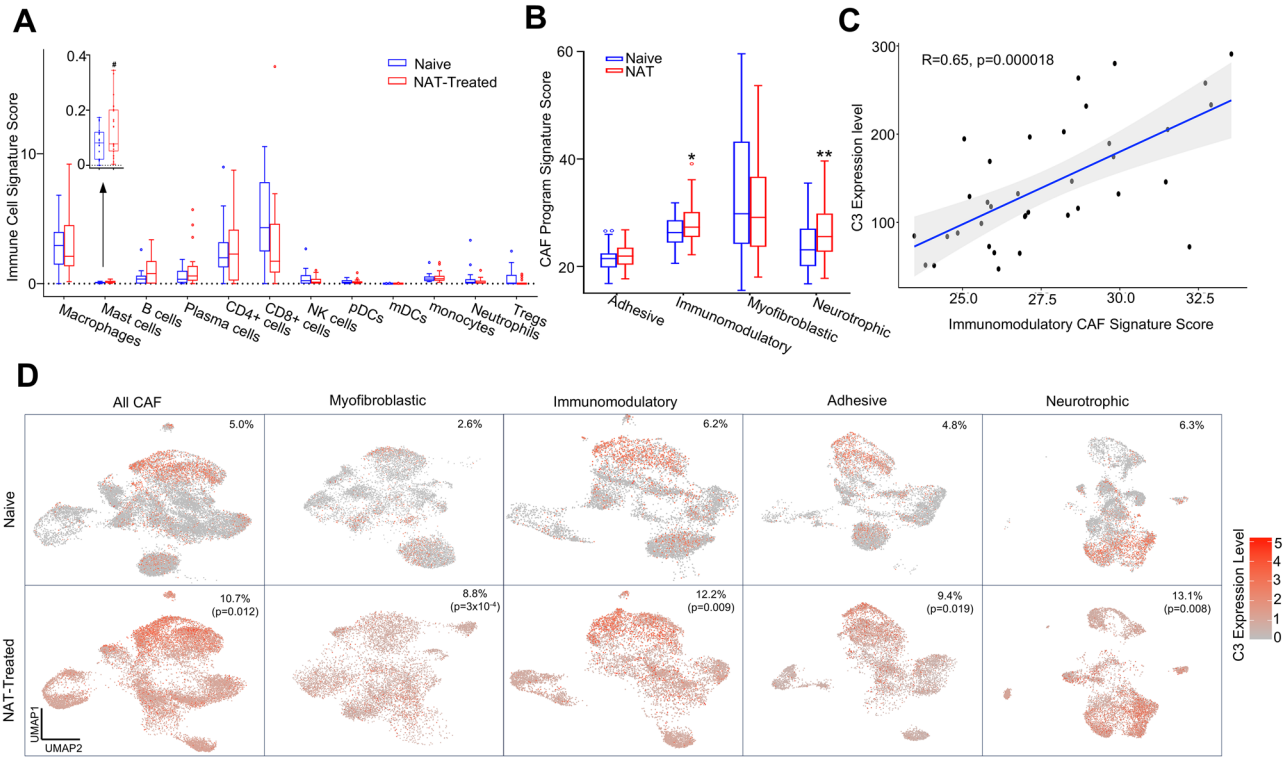


Fig. 4 | Impact of NAT on CAFs and immune cells in the TME of PDAC. **A** Quantitative analysis of signature scores for all major types of immune cell in the tumor immune microenvironment (TIME) in the naïve and NAT groups. No statistically significant changes were observed, except for a marginal increase in mast cell numbers. **B** NAT significantly increased immunomodulatory CAFs and the neurotrophic CAFs, with no significant changes observed in other CAF subtypes. **C** Complement C3 expression levels within TME are significantly correlated with the signature score of immunomodulatory CAFs (R = 0.65, p = 1.8e-5). **D** snRNA-seq analysis demonstrating a significant increase in the number of complement C3 expressing CAFs following NAT. The percentages of C3 expressing CAFs in each subtype and corresponding p-values are indicated in the upper right corner. (#$p < 0.1$; *$p < 0.05$; **$p < 0.01$).

signaling such as hsa04115 p53 signaling pathway (FDR = 1.73e-4). To illustrate the gene components for these enrichment terms, a chord map was made for the most significantly enriched functional terms and their related genes. The 5 complement genes (C1R, C1S, C3, C4B and C7) contribute to not only complement-related pathways, but also other key functional terms related to innate and adaptive immunity (Fig. 3B). These findings imply that NAT-induced upregulation of complement gene expression within TME may serve as a local regulatory hub in the TME and contribute to the overall immunomodulation in PDAC.

Next, we compared the gene expression profiles in the TME AOIs of the responders versus the non-responders in the NAT group. After controlling for age, gender and other clinicopathological factors, we identified 139 DEGs in responders when comparing to non-responders, including 62 up- and 77 downregulated genes (Fig. 3C, Supplementary Data 2). The most significantly upregulated genes include *HLA-DRB5* (p = 1.34e-4), *ILF3* (p = 1.15e-3) and *POLR2A* (p = 1.40e-3). The most significantly downregulated genes include *ITGB1* (p = 4.37e-4), *NTSE* (p = 8.40e-4) and *SIX1* (p = 5.28e-3). DAVID enrichment analysis indicated that the DEGs upregulated in the TME of the responders were significantly enriched with functional terms related with MHC Class II protein complex binding (enrichment fold = 58.60, FDR = 3.23e-4), Th1 and Th2 cell differentiation (enrichment fold=12.01, FDR = 6.64e-4) and Th17 cell differentiation (enrichment fold=13.15, FDR = 2.31e-5) (Fig. 3D). Interestingly, we found that the NAT-induced TME complement upregulation was only seen in responders but not in non-responders when compared to the naïve group (Fig. 3E). Enrichment analysis showed that while some pathways were enriched in both responders and non-responders (such as cellular senescence, p53 signaling and FoxO signaling), pathways related with complement activation and immunomodulation (such as MHC Class II protein complex binding, antigen processing and presentation, Th1/Th2 differentiation, and Th17 differentiation, etc.) were only enriched in responders (Fig. 3F). These findings suggest that complement upregulation may be associated with immunomodulation and treatment response.

To investigate how NAT influences the tumor immune microenvironment (TIME) in PDAC, signature scores for all major immune cell types were calculated for each TME AOI and tested for association with NAT while controlling age, gender, carcinoma grade and stage. There was no statistically significant change of signature scores for most types of immune cells in the TIME of the NAT group compared to the naïve group, except for mast cells which were increased with a marginal statistical significance (p = 0.09) (Fig. 4A). Next, we studied the effect of NAT on the cancer-associated fibroblasts (CAFs) using the expanded CAF classification system recently defined by Hwang et al. in 2022[25], in which CAFs are categorized into four specific programs based their gene expression profiles, including myofibroblastic, adhesive, immunomodulatory, and neurotrophic CAFs. We computed signature scores for all four programs of CAFs within each TME AOI and analyzed the association with NAT while controlling for age, gender, carcinoma grade and size. We found that immunomodulatory CAFs (p = 0.023) and neurotropic CAFs (p = 0.002) were significantly increased in the NAT group compared to the naïve group (Fig. 4B). To test what types of cells in the TME are responsible for the NAT-induced complement upregulation within TME, we studied the correlation between the expression level of C3, the most abundant complement component, and the signature scores for all major types of CAFs and immune cells. We found that the C3 expression level is most significantly correlated with the signature score of immunomodulatory CAFs (R = 0.65, p = 1.80e-5, Fig. 4C), suggesting that immunomodulatory CAFs are likely the major source of NAT-induced complement upregulation within TME.

To validate these findings of our spatial transcriptomics study, we analyzed a single-nucleus RNA (snRNA-seq) sequencing dataset from

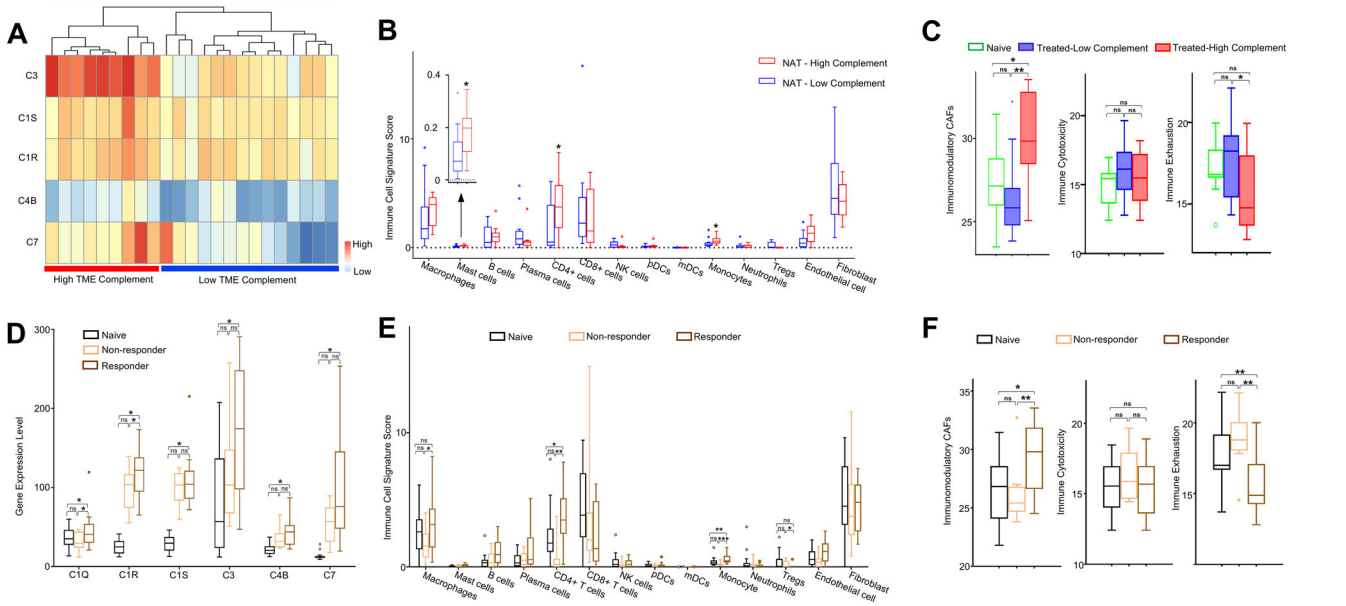


Fig. 5 | NAT-induced upregulation of complement expression in TME is associated with immunomodulation and reduced immune exhaustion. A Heatmap displaying the expression levels of the five key complement genes (C1R, C1S, C3, C4B, C7) that are upregulated by NAT in the TME of the NAT group. Unsupervised clustering segregates patients in NAT-group into high and low TME complement groups. **B** Box plot showing that the high TME complement subgroup has significantly increased numbers of mast cells, CD4 + T cells and monocytes compared to the low TME complement subgroup. **C** The high TME complement group exhibits significantly increased immunomodulatory CAFs compared to the low TME complement group. Additionally, the high TME complement subgroup shows significantly decreased immune exhaustion signature score and no significant change in immune cytotoxicity signature score. **D** Bar plot illustrating the expression levels of 5 complements (C1R, C1S, C3, C4B, C7) in the TME AOIs across the naïve group, the responder subgroup, and non-responder subgroup. **E** Box plot demonstrating that compared to the non-responder subgroup, the responder subgroup has significantly increased numbers of CD4 + T cells, monocytes and macrophages; and significantly decreased number of regulatory T (Treg) cells. **F** Responders show a significant increase in immunomodulatory CAFs compared to non-responders. Additionally, responders exhibit significantly decreased immune exhaustion signature scores and no significant change in immune cytotoxicity signature scores when compared to non-responders. (ns, not significant; $*p < 0.05$; $**p < 0.01$; $***p < 0.001$).

Hwang et al. [25], which was archived in the single cell portal. This dataset encompassed the gene expression profiles of 22,164 genes across 88031 cells from 15 NAT-naïve patients and 50516 cells from 11 NAT-treated patients. Our analysis revealed a significant increase of C3 expression in CAFs of the NAT-treated patients compared to NAT-naïve patients ($p = 0.044$). Based on generalized linear mixed model analysis, the proportion of C3 high expression CAFs was found to be significantly higher in NAT-treated patients than NAT-naïve patients, (10.66% vs. 5.03%, $p = 0.012$). (Fig. 4D). In contrast, no notable changes in C3 expression level were observed in other types of cells including carcinoma cells, immune cells and endothelial cells. A more detailed analysis on subtypes of CAFs showed that all subtypes of CAFs exhibited increased complement C3 gene expression, with the most pronounced increases observed in immunomodulatory and myofibroblastic CAFs. These results not only validated our spatial transcriptomics findings on NAT-induced C3 upregulation in a different cohort of patients, but also provided direct evidence that the CAFs represent the primary contributing cells of the complement gene expression upregulation in post-NAT TME.

NAT-induced upregulation of complement expression within TME is associated with immunomodulation and improved survival

To assess the clinical and prognostic significance of NAT-induced complement upregulation within TME, we stratified the NAT group into the high and low complement subgroups based on clustering analysis of the mean expression levels of the five complement genes upregulated in the post-NAT TME (C1R, C1S, C3, C4B, C7). Out of the 23 NAT-treated patients in our cohort, 9 were clustered into the high complement subgroup and 14 into the low complement subgroup (Fig. 5A). To elucidate how the upregulated complement expression regulates the tumor immune microenvironment, we compared the signature scores for all immune cells and CAF subtypes between the high and low complement subgroups of NAT-treated patients. Our results showed that the high complement subgroup exhibited significantly higher signature scores for mast cell ($p = 0.037$) and $CD4^+$ T cells ($p = 0.039$), as well as significantly higher signature scores for immunomodulatory ($p = 2.80e\text{-}3$) and neurotrophic subtypes of CAFs ($p = 3.6e\text{-}2$) compared to the low complement subgroup (Fig. 5B and C). In addition, the high complement subgroup also showed a notable reduction of expression for immune exhaustion gene signature ($p = 0.038$) while maintaining stable expression of immune cell cytotoxicity gene signature compared to the low complement subgroup (Fig. 5C). Further analysis using snRNA-seq data from Hwang et al.[25]. revealed reduced expression of immune checkpoint gene *CD274* (p = 0.019) and immune exhaustion gene *TIGIT* ($p = 0.034$) in NAT-treated patients compared to naïve patients. These results suggest that NAT-induced upregulation of complement gene expression within TME may lead to reduced immune exhaustion and immunosuppression in PDAC.

Next, we examined if treatment response is associated with NAT-induced upregulation of complement expression within TME. We found that NAT-induced upregulation of TME complement expression was only significant in the responders but not in the non-responders when compared to the naïve group (Fig. 5D). In addition to the 5 complement components (C1R, C1S, C3, C4B and C7) that were significantly upregulated when comparing the entire NAT group to the naïve group, C1QA, another component in the classical complement activation pathway, also showed significant upregulation when comparing only the responders to the naïve group (Fig. 5D). We then compared the signature scores for all major types of immune cells in the TME between responders and non-responders. In addition to significantly increased CD4 + T cells ($p = 0.0021$), the responders also exhibited significantly increased macrophages ($p = 0.037$) and monocytes ($p = 0.0003$), along with a significant decrease in Treg cells ($p = 0.043$) (Fig. 5E). Similarly, the responders showed significantly increased immunomodulatory CAFs, decreased immune exhaustion scores,

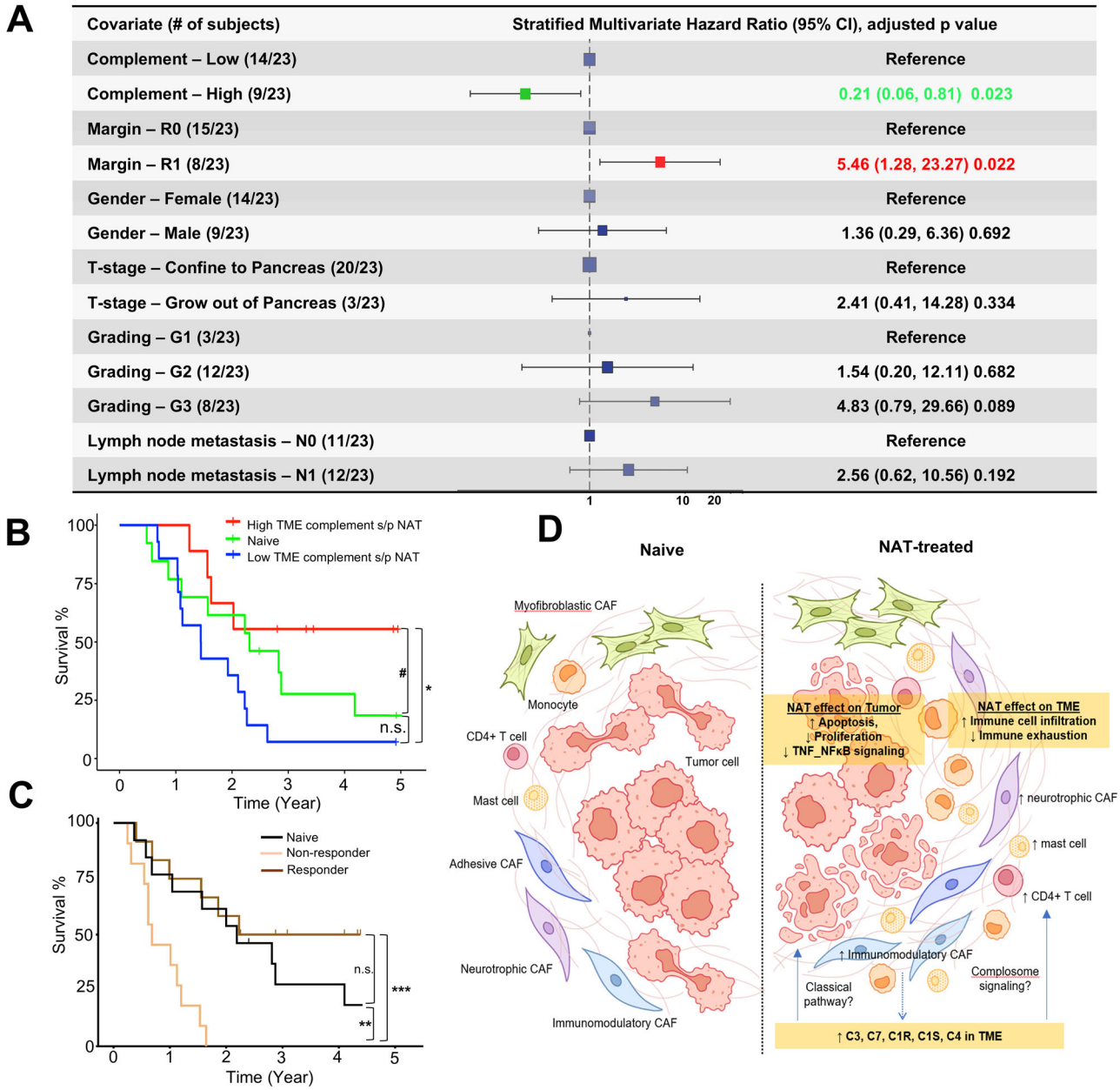


Fig. 6 | The prognostic relevance of NAT-induced upregulation of TME complement. A Forest plot of multivariate Cox proportional hazards analysis showing high TME complement level is an independent favorable prognostic factor for NAT-treated patients (HR = 0.21; 95% CI: 0.06-0.51; $p = 0.023$). Positive surgical resection margin (R1) is an independent poor prognostic factor for NAT-treated patients (HR = 5.46; 95% CI: 1.28-23.27, $p = 0.022$). **B** Kaplan-Meier survival curves comparing overall survival rates among the high TME complement subgroup (red line), the low TME complement subgroup (blue line) and the naïve group (green line). The high TME complement subgroup exhibits significantly improved overall survival compared to the low TME complement subgroup and marginally improved overall survival compared to the naïve group. No statistically significant difference was observed between the low TME complement subgroup and the naïve group. **C** Kaplan-Meier survival curves comparing the overall survival among the responder group (dark brown), the non-responder group (light brown) and the naïve group (black). The responders showed significantly improved overall survival compared to the non-responders. No statistically significant difference was observed in overall survival between the responders and the naïve group. **D** Schematic representation summarizing how NAT differentially remodels carcinoma cells and the TME of PDAC. While NAT increases apoptosis and decreases the proliferation and G2/M phase cycling in carcinoma cells, it has broad immunomodulatory effects on the TME through upregulating local complement expression and signaling. (ns, not significant; #$p < 0.1$; *$p < 0.05$; **$p < 0.01$; ***$p < 0.001$).

and similar immune cytotoxicity scores when compared to the non-responders (Fig. 5F).

To investigate the clinical and prognostic significance of complement-mediated immunomodulation, we conducted a multivariate Cox proportional hazard ratio analysis. This analysis identified a high TME complement level as an independent favorable prognostic factor for NAT-treated patients (hazard ratio = 0.21; 95% Confidence Interval (CI): 0.06 to 0.81, $p = 0.023$) (Fig. 6A). In contrast, a positive surgical resection margin (R1) was recognized as an independent adverse prognostic factor (HR = 5.45, 95% CI = 1.28-23.27) (Fig. 6A). Kaplan-Meier analysis indicated that the high complement subgroup demonstrated a significantly better overall survival compared to the low complement subgroup ($p = 0.023$) and showed a marginally better survival trend compared to the naïve group ($p < 0.1$). The survival rates of the low complement subgroup rates were not significantly different from those of the naïve group (Fig. 6B). Additionally, while the responders to NAT exhibited significantly better overall survival than the

non-responders ($p = 0.0006$), its overall survival was not significantly different from that of the naïve group. In contrast, the non-responders exhibited significantly worse overall survival than both the responders and the naïve group ($p = 0.0016$) (Fig. 6C).

To further clarify the link between the elevated complement expression in TME and survival benefits in post-NAT patients, we also conducted a longitudinal paired analysis of complement C3 level in the TME of the four patients for whom we had both pre-NAT biopsy and post-NAT resection samples. We examined the changes in TME C3 expression levels and their correlation with clinical outcomes. Among these 4 patients, two of them displayed a significantly increased TME C3 expression level following NAT and showed improved overall survival compared to the rest two patients who did not show an increase in TME C3 level post-NAT (Supplementary Fig. 4). These results imply that patients with a significant upregulation of TME complement level in response to NAT could be indicative of an improved overall survival.

Discussion

Our results revealed that NAT differentially remodels the carcinoma cells and the TME of PDAC through distinct mechanisms. By comprehensively comparing the spatial transcriptomic profiles of more than 1800 genes related to cancer biology, TME and immune responses between a sizable cohort of patients treated with NAT versus those who were NAT-naïve, we demonstrated that NAT induced 44 DEGs in carcinoma cells and 52 DEGs in the TME. Gene set enrichment (GSE) analysis revealed nine significantly up- or downregulated gene sets and functional terms in NAT-treated carcinoma cells, compared to 61 in NAT-treated TME. These results indicate that NAT may exert a more extensive and profound remodeling effect on the TME than on the carcinoma cells per se. In NAT-treated carcinoma cells, most DEGs are associated with apoptosis regulation, cell cycle control, and DNA repair. Among them, the most significantly upregulated DEG was *DDB2* ($p = 0.00077$), which encodes DNA damage-binding protein 2, a nuclear protein crucial for DNA repair and genomic stability. Additionally, DDB2 has been shown to suppress epithelial-to-mesenchymal transition (EMT) and enhance sensitivity to chemotherapy in PDAC[39]. Conversely, in the TME of NAT-treated PDAC, most DEGs are associated with complement signaling and regulation of innate and adaptive immune function. Among them, the most significantly downregulated DEG was *HDAC2*, which encodes histone deacetylase 2, a transcription factor capable of inducing inflammatory gene expression in CAFs and supporting carcinoma growth in PDAC. Recent studies have demonstrated the role of HDAC2 in facilitating pancreatic cancer metastasis[40].

Notably, we observed a coordinated upregulation of five key complement genes (C3, C4B, C7, C1R, C1S) in the TME of NAT-treated PDAC as compared to those not treated by NAT. Due to the collective upregulation of these five complement genes, the complement pathway emerged as the most significantly enriched pathway (FDR = 1.04×10^{-5}) among the NAT upregulated gene sets. It is worth emphasizing that this NAT-induced upregulation of complement expression was spatially confined to TME. Traditionally, complement proteins were primarily considered to be produced in the liver and circulating in the bloodstream to aid the immune function by opsonization[41]. However, our results suggest that the complements may also be produced locally within TME and play an important role in regulating immune response. Analysis of snRNA-seq data validated our spatial transcriptomics findings, and pinpointed CAFs as the primary mediators of this NAT-induced upregulation of complement within TME, while complement gene expression in carcinoma cells and immune cells was not notably changed. As fibroblasts are the most abundant cell type in TME, our results suggest that CAFs are likely the main factor contributing to the local production of complement proteins within the TME of PDAC.

Our findings align with several recent single-cell or single-nucleus RNA-sequencing (sc/snRNA-Seq) studies. In 2021, Chen et al. identified a distinctive subtype of CAF, which they named "complement-secreting CAFs" (cs-CAFs), characterized by their enrichment with complement system genes. They found that cs-CAFs were predominantly located near malignant glands, and mainly existed in early-stage and diminished in late-stage PDAC[42]. Recently, Croft et al. demonstrated that some CAFs located more distant from malignant glands can also produce complement proteins, and their increase was associated with improved patient survival[43]. In 2022, Hwang et al.[25] expanded the CAF classification system to include four subtypes: myofibroblastic, adhesive, immunomodulatory, and neurotrophic. They noted an overlap between the latter three subtypes and the previously defined inflammatory type CAFs. They also showed that immunomodulatory CAFs are enriched with complement genes[25]. Similarly, Werba et al. also observed complement gene enrichment in inflammatory CAFs[34]. However, none of these sc/snRNA-Seq studies specifically investigated the impact of NAT on complement gene expression within TME. Our research, for the first time, demonstrated a NAT-induced upregulation of complement expression in CAFs. Further studies, especially those using single-cell spatial transcriptomics, are warranted to characterize how NAT influences the spatial distribution and adaptability of different subtypes of CAFs. A recent study by Shiau et al. using single-cell spatial transcriptomics revealed that NAT induced significant changes in the interaction strength between malignant cells and inflammatory CAFs mediated by enriched IL-6ST[31]. Correspondingly, our study also showed a significant upregulation of IL-6ST expression in post-NAT TME, contributing to the regulation of immune function (Figs. 3A, C, D). Taken together, these results suggest that NAT can substantially remodel the TME and influence the interplay between carcinoma cells and CAFs.

Another interesting finding of our study is that NAT-induced upregulation of complement expression within TME is associated with modulation of the TIME and decreased expression of immune exhaustion markers, as demonstrated in our spatial transcriptomics analysis (Fig. 5C) and validated by the snRNA-seq data. Importantly, the NAT-treated patients with higher complement expression within TME demonstrated improved overall survival (Fig. 6B). The detailed cellular and molecular mechanisms underlying these observations remain to be further elucidated. It is known that some cleaved complement proteins (such as C3a, C5a, etc.) are potent chemoattractant and can recruit immune cells into TIME[44–46]. Recent evidence also indicated that a tonic level of complements in the microenvironment is required for maintaining immune cell homeostasis and function via the non-canonical intracellular complement (i.e., complosome) signaling[47,48]. For example, studies by Arbore et al., have demonstrated an essential role of CD46-mediated intracellular complement signaling in regulating Th1 cell life cycle[49] and CD8 + T cell effector function[50]. In our study, we also found that the interaction strength between CD46 and complement C3 was significantly increased in the high complement subgroup as compared to the low complement subgroup ($p = 2e\text{-}8$) and the naïve groups ($p = 4e\text{-}6$). Furthermore, the high complement subgroup showed significant enrichment of the Th1/Th2 cell differentiation pathway, as compared to the naïve group (enrichment fold =13.7, $p = 4e\text{-}4$, FDR=2e-3). This enrichment was not observed when comparing the low complement subgroup to the naïve group. These results suggest that a similar complosome signaling mechanism, as demonstrated by Arbore et al.[49] may be involved in regulating the life cycle of Th1 cells in the TME of NAT-treated PDAC. These findings suggest that TME complement may serve as a regulatory hub for innate and adaptive immune functions via canonical and non-canonical signaling mechanisms. Future studies using single-cell spatial RNA sequencing to more accurately quantify Th1 cells within TME would greatly enhance our understanding of how local complement influences the dynamics of CD4 + T cell differentiation within TME.

Our study is the first spatial transcriptomics study specifically aimed at comparing the differential remodeling effect of NAT on carcinoma cells and the TME using FFPE tissue of primary PDAC. The cohort size is relatively limited, yet comparable to multiple scRNA-seq studies recently published in the field [23,25,34,42,43,51]. The main limitation of our approach is that the spatial transcriptomics method used here cannot achieve single-cell resolution. The digital micromirror device (DMD) used by the Nanostring GeoMx DSP system for segmentation provides an optical spatial resolution of 10

microns. While this resolution is typically sufficient for separating most carcinoma and TME AOIs defined in our study (all of which contained at least 100 cells), the heterogeneity of PDAC can sometimes make an accurate segmentation challenging[21]. For example, PDAC can exhibit areas with highly convoluted tumor-stroma interface; sometimes even single or small clusters of PDAC cancer cells buried in abundant dense desmoplastic stroma[52]. On the other hand, carcinoma AOIs may be infiltrated by immune cells, such as tumor-infiltrating lymphocytes (TILs), tumor-associated macrophages (TAMs), or neutrophil extracellular traps (NETs), further complicating precise segmentation. These features can result in mixed signals from both carcinoma and TME AOIs, leading to the formation of an intermingled cluster. Additionally, although not common, PDAC cells may undergo epithelial-mesenchymal transition and exhibit characteristics more closely resembling those of the TME[53]. This could also potentially cause them to cluster more closely with TME AOIs in the UMAP space. These technical and biological factors may contribute to the suboptimal separation of a minority of carcinoma and TME AOIs in our study, shown as a partial overlap at the tails of the carcinoma and TME AOI clusters in the UMAP space (Fig. 1D). This is a typical example that calls for the high dimensional multiplex immunohistochemistry and single-cell spatial RNA sequencing for more definitive and accurate characterization of PDAC in its intact microenvironment.

On the other hand, since there is no cell isolation and processing needed as in single-cell or single-nucleus RNA-seq, the method used in our study reduces technical variability and batch effect and is not impacted by the artifactual transcriptomics changes due to the procedure-induced cell stress. This is especially important for PDAC in which all cellular components are buried in excessive dense extracellular matrix which makes cell isolation particularly challenging. In addition, by pooling mRNAs from each AOI, this method can achieve higher mRNA concentration per sample, thus facilitating deeper sequencing and reduced dropouts, thereby enhancing the signal-to-noise ratio. Consequently, it enables more robust detection of weakly expressed genes. Recently, the scRNA-seq study by Werba et al. observed generally decreased cell-cell interaction and high volume of putative interactions between CAFs and tumor-associated macrophages (TAMs) in the TME of NAT-treated PDAC[34]. No difference was noted in CAF subpopulation distributions between NAT-treated vs. naive groups[34]. Hwang et al. discovered that NAT could increase the adhesive CAFs and decrease the myofibroblast CAFs. They also found that the number of immunomodulatory CAFs was higher in patients treated with regular NAT than those with NAT plus losartan[25]. In the most recent study using single-cell spatial transcriptomics, Shiau et al. showed a marked increased ligand-receptor interaction between CAFs and malignant cells in NAT-treated PDAC[31]. Therefore, our data have not only confirmed previous sc/snRNA-seq studies but also provided additional valuable insights thanks to the preserved spatial context.

The interesting findings from our study call for further investigations on the molecular mechanisms by which local complement signaling modulates immune cells functions within TME. The complement system plays a pivotal role in regulating both innate and adaptive immune functions in inflammatory and neoplastic conditions through both canonical and non-canonical pathways. For instance, Kumar S. et al. demonstrated that adventitial fibroblasts activated by pulmonary hypertension could release complement proteins through paracrine secretion of extracellular vesicles, subsequently reprogramming macrophage metabolism[54]. In addition, Arbore G et al., demonstrated that intracellular complement signaling was crucial for regulating both the Th1 cell life cycle and CD8 + T cell effector function[49,50]. Under neoplastic condition, studies have shown that chemotherapy can enhance extracellular vesicle release of complement proteins in breast cancer models and paradoxically increase the risk of lung metastasis[55,56]. On the other hand, other studies demonstrated that complement was a central mediator of radiotherapy-induced anti-tumor immunity[57]. These studies highlight the dual functionality of complement signaling as a double-edge sword. Further research is needed to gain deeper understanding of the context-dependent effect of complement signaling on tumor and immune cells within TME. Such knowledge could pave the way for new therapeutic strategies that target the dynamics of local complement.

In conclusion, by using spatially resolved transcriptomics, we demonstrated that NAT remodels the carcinoma cells and the TME of PDACs through different mechanisms. NAT can significantly upregulate complement gene expression within TME, which is associated with immunomodulation and improved survival. These results suggest that NAT may potentially attenuate immune cell exhaustion and enhance immune surveillance in some PDAC patients by upregulating local complement production and signaling. Those patients who did not respond to NAT with a significant upregulation of TME complement may have more immune exhaustion and thus benefit from combinational immune checkpoint blockade therapy. Therefore, assessment of the local complement dynamics in the TME may provide more accurate prognostic guidance for NAT-treated patients, which may help to stratify them for more tailored downstream interventions. Further analyses, especially single-cell spatial transcriptomics within intact spatial context, are warranted to further elucidate the detailed cellular and molecular mechanisms of complement-mediated immunomodulation and its potential therapeutic implications.

Methods

Patient cohort and data collection

This study was performed in accordance with the Declaration of Helsinki. The study protocols were approved by the Institutional Review Boards at University of Wisconsin—Madison (IRB#2018-1510, Protocol UW18144) and New York University Grossman Long Island School of Medicine (i23-00536). As this is a purely retrospective and observational study and only used tissue sections cut from archived formalin-fixed, paraffin-embedded (FFPE) tissue block without utilizing any fresh tissue from any human research participants, the requirement for informed consent was waived by the institutional ethics committees. All slides were de-identified before whole slide scanning. We retrospectively reviewed PDAC patients who underwent surgical resection at UW-Madison between 2015 to 2020. To protect patient privacy and confidentiality, all clinical data collection protocols were reviewed and approved by Institutional Review Boards (see protocol numbers above). The inclusion criteria were PDAC patients aged 18–80 years from both genders. Patients with incomplete clinicopathologic information or those with incomplete archived slides or blocks were excluded. From this review, 36 patients were identified as meeting the study criteria, including 23 patients who had NAT (either chemotherapy alone or in combination with radiation) before surgery, and 13 patients who underwent upfront surgical resection without any forms of NAT who were selected using case-control matching to ensure statistical control over any potentially confounding clinicopathologic variables, such as age, gender, tumor size, grading etc. Chi-squared test showed no statistically significant differences in any of these factors between the NAT and the naïve groups (Supplementary Table 1). The response to NAT treatment was graded by histopathologic evaluation based on the American Joint Committee on Cancer/College of American Pathologists Tumor Regression Grading system (AJCC/CAP-TRG). The pertinent clinicopathological information was retrospectively collected by reviewing electronic medical records under the IRB-approved protocols. These data were de-identified prior to analysis. Among the 23 patients in the NAT group, 17 patients received multiple cycles of FOLFORINOX, and 6 patients received multiple cycles of gemcitabine and Abraxane. Nine patients received concurrent radiation therapy. For all patients, only resection specimens were used, except for 4 patients, for whom the pre-NAT biopsies were also included for a paired comparison with their corresponding post-NAT resection specimen.

Sample preparation for NanoString GeoMx DSP

Serial sections (4-μm in thickness) were cut from the selected formalin-fixed, paraffin-embedded (FFPE) tissue block for the consecutive H&E staining and immunofluorescence staining for DSP (Digital Spatial Profiler) experiment. For DSP experiment, sections were baked at 60 °C for 1.5 h and deparaffinized in CitriSolv. fter rehydration, sections were incubated in

100 °C 1xTris-EDTA/pH9 buffer for 15 min for antigen retrieval. After digestion and post-fixation, all sections were hybridized to UV-photocleavable barcode-conjugated RNA in situ hybridization probe set (Nanostring CTA, 1812 gene targets) overnight at 37 °C. Then, all slides were washed to remove off-target probes. Next, slides were used for immunofluorescence staining with morphology markers set, which contains 1:10 SYTO13 (Thermo Fisher Scientific, cat. no. 57575), 1:20 anti-panCK-Alexa Fluor 532 (clone AE-1/AE-3; Novus Biologicals, cat. no. NBP2-33200AF532), and 1:100 anti-αSMA-Alexa Fluor 647 (clone 1A4; Novus Biologicals, cat. no. IC1420R) in blocking buffer (NanoString). For each slide, 2–5 ROIs (Regions of Interest) with the most representative morphology were selected. Each ROI was segmented into carcinoma AOI (area of illumination, panCK+, SMA-) and TME AOI (panCK-, SMA+) using the scanned immunofluorescence image. Photocleavage of spatially indexed barcode and sample collection were done on GeoMx DSP equipment (NanoString). Samples obtained from each AOI were collected in a 96-well plate. RNA Libraries were prepared according to the manufacturer's instructions. Then, Next Generation Sequencing (NGS) read-out was done using an Illumina NextSeq 550AR sequencer. The data was exported as digital count conversion (DCC) files which were used for analysis using R and Bioconductor packages.

Data pre-processing and normalization

We followed a published online R and Bioconductor GeoMx-NGS workflow (NanoString Technologies, Inc) for QC (quality control), pre-processing and normalization of raw GeoMx DSP count files and metadata. The website of the workflow is https://bioconductor.org/packages/devel/workflows/vignettes/GeoMxWorkflows/inst/doc/GeomxTools_RNA-NGS_Analysis.html. In brief, the workflow included data loading (DCC, PKC and annotation files) and illustration of study design using Sankey diagram (Supplementary Figure 1). The loaded data then underwent QC and pre-processing steps, including segment QC for every AOI segment (e.g., removing segments with >1000 raw reads and those with less than 80% rate for aligned percentage, trimmed percentage or stitched percentage), probe QC to remove low-performing probes, creation of gene-level count data by combining counts across multiple probes of a gene via geometric mean, and determination of limit of quantification (LOQ) of each segment based on the distribution of negative control probes. Based on the calculated LOQ, the number of detected genes was decided for each segment. Segment-wise gene detection rate was inferred, and those segments with less than 1% of gene detection rate were removed. Similarly, the detection rate for each gene across the study was determined and those genes detected in <5% of all segments were removed. Based on the filtered gene expression matrix, the GeoMx data were normalized using Q3 (3rd quartile) normalization. The Q3 normalized data were then used for downstream data analyses.

Unsupervised analysis

The UMAP method was used to visualize the segment-level data in two major dimensions (UMAP1 and UMAP2) by using the UMAP R package. Unsupervised hierarchical clustering of all genes was performed using pheatmap package by first conducting log2 transformation of the data, followed by selecting highly variable genes (i.e., those of top 20 percentile of coefficient of variation of gene expression) to be included in the cluster heatmap. Similarly, unsupervised hierarchical clustering of 5 complement genes (C3, C1S, C1R, C4B and C7) was performed with the pheatmap package using subject-wise average of gene expression values of these 5 complement genes in the TME.

Differential expression analysis

Linear modeling analysis implemented in R was conducted to detect the effect of NAT on gene expression profiles in either the carcinoma cells AOIs or the TME AOIs. Specifically, the log2 transformed subject-wise average of gene expression of carcinoma AOIs or the TME AOIs was modeled as the dependent variable, with independent variables including treatment status (i.e., NAT vs. naïve), age, gender, pathology grade and size of the tumor. The estimate and the p value for the regression coefficient for treatment status (NAT-treated vs. naïve) were used to represent the effect of differential expression induced by NAT. To illustrate the differential expression, volcano plots were made with EnhancedVolcano package (version 1.13.2).

Signature scores for immune and fibroblast cell types

Signature scores for immune cell types of each AOI were computed from the gene expression matrix with SpatialDecon package (version 1.4.3). Scores for other signature scores, including Malignant State Programs (i.e., cycling (S), cycling (G2/M), MYC signaling, adhesive, ribosomal, interferon signaling and TNF-NFkB signaling), Malignant Lineage Program (i.e., acinar-like, classical-like, basaloid, squamoid, mesenchymal, neuroendocrine-like, neural-like progenitor) and Fibroblast Programs (i.e., adhesive, immunomodulatory, myofibroblastic and neurotropic) were inferred based on geometric average of signature genes as described by Hwang et al. in 2022[25]. The signature score for Immune Exhaustion was inferred from the signature genes as provided in Werba et al., in 2023[34] (Supplementary Note 1). The SpatialDecon R package[58] was used to compute the signature score of immune cells (i.e., mast cells, CD4+ cells, CD8+ cells etc.) using the quantile normalized gene expression matrix. The same linear modeling analysis was used to test the effect of NAT on the above-inferred signature scores.

Gene set enrichment analysis

The differentially expressed genes with p value < 0.05 were submitted to DAVID enrichment analysis portal (https://david.ncifcrf.gov/home.jsp) for gene set enrichment analysis[59,60]. To infer up- or downregulated gene sets, the up- or downregulated genes were submitted for analysis separately. To visualize the enriched gene sets, dot plots were made with ggplot2 R package (v3.4.2) and chord maps were plotted with GOplot package (v1.0.2).

Survival analysis

R packages, survival (v3.5.5) and survminer (v0.4.9), were used to make Kaplan Meier (KM) survival curve and compare and test significance for the difference of survival between different groups of patients. The Cox Proportional Hazards Model was used to test the significance of survival differences in groups of patients while controlling for age, gender, tumor size, and cancer grading.

Single-cell nucleus RNA-seq data analyses

Single-nucleus RNA-seq (snRNA-seq) data of Hwang et al.[25]. was downloaded from Single Cell Portal at https://singlecell.broadinstitute.org/single_cell/study/SCP1089 (for 88031 naïve cells from 15 NAT-naïve PDAC patients) and https://singlecell.broadinstitute.org/single_cell/study/SCP1096 (for 50,516 treated cells in 11 NAT-treated patients). For the purpose of this study, we only downloaded the snRNA-seq data of the already annotated fibroblasts, carcinoma cells, and immune cells.

We used Seurat pipeline[61,62] for the initial processing and analyses of the downloaded data. The major analyses involved data merging of treated and naïve dataset, data normalization, identification of 2000 most variable genes, dimensionality reduction and visualization of gene expression in UMAP plots and highlighting and comparing between treated and naïve groups for expression of important genes, such as C3, in specific cell populations within UMAP plots.

To annotate and define subtypes of CAFs, signature genes of each specific groups as described in Hwang et al.[25] were used. Specifically, if a cell's signature gene score for a subtype is higher than the cell's background gene score, the cell will be assigned to this subtype. For a given cell, the signature or background gene score was calculated via the mean of log2 transformed gene expression values of all genes in different gene signatures. The background gene set was determined by selecting those genes that matched with individual signature genes in terms of ranks of the across-cell mean expression (i.e., the mean log2 expression) among all expressed genes in CAFs.

A linear mixed model was used to compare a gene's expression in NAT-treated vs. naïve patients via lme4 package in R. The model was constructed as: [log2(GE) ~ treatment + (1|subject)], which accounted for subject-level random effects. Similarly, using MASS library in R, a generalized linear mixed model was used to compare the proportion of C3 high-expression cells in NAT-treated vs. NAT-naïve patients. The model was constructed as: [C3 high-expression cells ~ Treatment, random = ~1|subject, family = binomial]. Here, a C3 high-expression cell was defined as a cell with a C3 expression level above the median of all non-zero cells. A similar approach with generalized linear mixed model was taken to compare NAT-treated vs. NAT-naïve patients for the proportion of immune cells with a high expression of immune exhaustion genes (CD274, CTLA4, HAVCR2, LAG3 and TIGIT), with the median of non-zero cells as the cutoff to define the cells of high expression for the above genes. For the above analyses, one-tailed p values were used since the analyses were based on the hypotheses that there is increased complement gene expression in fibroblasts and increased fibroblasts with a high expression of complement genes in NAT-treated patients than naïve-treated patients. Within immune cells, our hypothesis is that there is a decreased expression of immune exhaustion genes in NAT-treated patients than naïve patients.

Other analyses

Linear mixed modeling using lme4 package in R was performed to model the immune cell signature score in an AOI as the dependent variable and C3 expression in the same AOI as the independent variable, and the model's regression coefficient (estimated as the fixed effects) may represent the spatial correlation between the two variables. Additionally, the variation of the regression line's intercept across different patients was modeled as random effects. Specifically, the model was constructed as: [immune cell signature score in an AOI ~ C3 level in the same AOI + (1|subject)], which accounted for subject-level random effects.

Ligand-receptor interaction analysis (C3 × CD46) was performed following the method as described by Lin et al. in 2021 (Lin et al. Journal of Translational Medicine (2021) 19:497)[63]. Specifically, the product of mean TME expression levels of C3 and CD46 was calculated. The significance of the product was assessed through a permutation process, where a pair of genes was randomly selected with the product of their expression values calculated and such procedure was repeated for 2000 times, with all the computed products of gene expression values ($n = 2000$) compiled into a null distribution. The significance of the product of gene expression values of C3 and Cd46 was assessed against the null distribution, with the statistical significance (the empirical p value) computed as the upper percentile achieved.

To test for interaction strength of C3 and CD46, the product of C3 and CD46 expression values was calculated for each subject and linear modeling analysis was performed to compare that product values (log2 transformed) in different groups, controlling for key clinical covariates (age, gender, cancer grading and tumor size).

We calculated the coefficient of variation (CoV) of expression levels for each gene across different AOIs from the same subject. The assessment was performed separately for carcinoma and TME AOIs in both naïve and treated groups. To describe the central tendency as well as the dispersion of CoVs for each gene in each of the four subgroups (i.e., naïve carcinoma AOIs, treated carcinoma AOIs, naïve TME AOIs, treated TME AOIs), we computed the median, 1st and 3rd quartile of CoV values for each gene across that subgroup. These results are presented in Supplementary Figs. 5. The (subject-wise) medians of CoVs for most genes (93.7–97.4%) are less than 0.3. Furthermore, for 72.73% to 86.36% of genes, the (subject-wise) 3rd quartile of CoVs was under 0.3. These results indicate that the CoVs were generally quite low for most genes across all these four sub-groups. Importantly, the variation was similar in scale between naïve and treatment groups, as well as between carcinoma and TMI AOIs.

Data availability

The spatial transcriptomics data used here along with the metadata were submitted to NCBI GEO (Gene Expression Omnibus) with an accession number of GSE240078.

Code availability

All code used for data processing and analysis in this study is provided as Supplementary Data 3. R version 4.1.2 was used for all data analyses. Detailed information regarding all software versions and specific analysis parameters is provided in the Supplementary Information.

Received: 14 March 2024; Accepted: 24 February 2025;
Published online: 03 March 2025

References

1. Siegel, R. L., Miller, K. D., Fuchs, H. E. & Jemal, A. Cancer statistics, 2022. *CA Cancer J. Clin.* **72**, 7–33 (2022).
2. Rahib, L., Wehner, M. R., Matrisian, L. M. & Nead, K. T. Estimated projection of US cancer incidence and death to 2040. *JAMA Netw. Open* **4**, e214708 (2021).
3. Vincent, A., Herman, J., Schulick, R., Hruban, R. H. & Goggins, M. Pancreatic cancer. *Lancet* **378**, 607–620 (2011).
4. Ferrone, C. R. et al. Pancreatic adenocarcinoma: the actual 5-year survivors. *J. Gastrointest. Surg.* **12**, 701–706 (2008).
5. Hu, Z. I. & O'Reilly, E. M. Therapeutic developments in pancreatic cancer. *Nat. Rev. Gastroenterol. Hepatol.* **21**, 7–24 (2024).
6. Wood, L. D., Canto, M. I., Jaffee, E. M. & Simeone, D. M. Pancreatic cancer: pathogenesis, screening, diagnosis, and treatment. *Gastroenterology* **163**, 386–402.e381 (2022).
7. Manrai, M., Tilak, T., Dawra, S., Srivastava, S. & Singh, A. Current and emerging therapeutic strategies in pancreatic cancer: challenges and opportunities. *World J. Gastroenterol.* **27**, 6572–6589 (2021).
8. Collisson, E. A., Bailey, P., Chang, D. K. & Biankin, A. V. Molecular subtypes of pancreatic cancer. *Nat. Rev. Gastroenterol. Hepatol.* **16**, 207–220 (2019).
9. Herting, C. J., Karpovsky, I. & Lesinski, G. B. The tumor microenvironment in pancreatic ductal adenocarcinoma: current perspectives and future directions. *Cancer Metastasis Rev.* **40**, 675–689 (2021).
10. Shibuya, K. C. et al. Pancreatic ductal adenocarcinoma contains an effector and regulatory immune cell infiltrate that is altered by multimodal neoadjuvant treatment. *PLoS One* **9**, e96565 (2014).
11. Hosein, A. N., Brekken, R. A. & Maitra, A. Pancreatic cancer stroma: an update on therapeutic targeting strategies. *Nat. Rev. Gastroenterol. Hepatol.* **17**, 487–505 (2020).
12. Su, H. et al. Collagenolysis-dependent DDR1 signalling dictates pancreatic cancer outcome. *Nature* **610**, 366–372 (2022).
13. Murphy, J. E. et al. Total neoadjuvant therapy With FOLFIRINOX followed by individualized chemoradiotherapy for borderline resectable pancreatic adenocarcinoma: a phase 2 clinical trial. *JAMA Oncol.* **4**, 963–969 (2018).
14. Versteijne, E. et al. Neoadjuvant chemoradiotherapy versus upfront surgery for resectable and borderline resectable pancreatic cancer: long-term results of the Dutch randomized PREOPANC trial. *J. Clin. Oncol.* **40**, 1220–1230 (2022).
15. Attaallah, W. Neoadjuvant chemoradiotherapy for resectable and borderline resectable pancreatic cancer. *J. Clin. Oncol.* **40**, 3346 (2022).
16. Krishnamoorthy, M., Lenehan, J. G. & Maleki Vareki, S. Neoadjuvant immunotherapy for high-risk, resectable malignancies: scientific rationale and clinical challenges. *J. Natl Cancer Inst.* **113**, 823–832 (2021).
17. Patel, R. B. et al. Low-dose targeted radionuclide therapy renders immunologically cold tumors responsive to immune checkpoint

blockade. *Sci. Transl. Med.* **13**, https://doi.org/10.1126/scitranslmed.abb3631 (2021).
18. Kuipers, J., Jahn, K. & Beerenwinkel, N. Advances in understanding tumour evolution through single-cell sequencing. *Biochim. Biophys. Acta Rev. Cancer* **1867**, 127–138 (2017).
19. Lahnemann, D. et al. Eleven grand challenges in single-cell data science. *Genome Biol.* **21**, 31 (2020).
20. Ali, L. R. et al. PD-1 blockade induces reactivation of non-productive T cell responses characterized by NF-kB signaling in patients with pancreatic cancer. *Clin. Cancer Res*. https://doi.org/10.1158/1078-0432.CCR-23-1444 (2023).
21. Barthel, S., Falcomata, C., Rad, R., Theis, F. J. & Saur, D. Single-cell profiling to explore pancreatic cancer heterogeneity, plasticity and response to therapy. *Nat. Cancer* **4**, 454–467 (2023).
22. Chen, K. et al. Single-cell RNA-seq reveals characteristics in tumor microenvironment of PDAC with MSI-H following neoadjuvant chemotherapy with anti-PD-1 therapy. *Cancer Lett.* **576**, 216421 (2023).
23. Cui Zhou, D. et al. Spatially restricted drivers and transitional cell populations cooperate with the microenvironment in untreated and chemo-resistant pancreatic cancer. *Nat. Genet.* **54**, 1390–1405 (2022).
24. Han, J., DePinho, R. A. & Maitra, A. Single-cell RNA sequencing in pancreatic cancer. *Nat. Rev. Gastroenterol. Hepatol.* **18**, 451–452 (2021).
25. Hwang, W. L. et al. Single-nucleus and spatial transcriptome profiling of pancreatic cancer identifies multicellular dynamics associated with neoadjuvant treatment. *Nat. Genet.* **54**, 1178–1191 (2022).
26. Kinker, G. S. et al. Mature tertiary lymphoid structures are key niches of tumour-specific immune responses in pancreatic ductal adenocarcinomas. *Gut* **72**, 1927–1941 (2023).
27. Li, K. et al. Multi-omic analyses of changes in the tumor microenvironment of pancreatic adenocarcinoma following neoadjuvant treatment with anti-PD-1 therapy. *Cancer Cell* **40**, 1374–1391.e1377 (2022).
28. Lin, W. et al. Single-cell transcriptome analysis of tumor and stromal compartments of pancreatic ductal adenocarcinoma primary tumors and metastatic lesions. *Genome Med.* **12**, 80 (2020).
29. Peng, J. et al. Single-cell RNA-seq highlights intra-tumoral heterogeneity and malignant progression in pancreatic ductal adenocarcinoma. *Cell Res.* **29**, 725–738 (2019).
30. Raghavan, S. et al. Microenvironment drives cell state, plasticity, and drug response in pancreatic cancer. *Cell* **184**, 6119–6137.e6126 (2021).
31. Shiau, C. et al. Therapy-associated remodeling of pancreatic cancer revealed by single-cell spatial transcriptomics and optimal transport analysis. *bioRxiv*, https://doi.org/10.1101/2023.06.28.546848 (2023).
32. Shiau, C. et al. Treatment-associated remodeling of the pancreatic cancer endothelium at single-cell resolution. *Front Oncol.* **12**, 929950 (2022).
33. Ting, D. T. et al. Single-cell RNA sequencing identifies extracellular matrix gene expression by pancreatic circulating tumor cells. *Cell Rep.* **8**, 1905–1918 (2014).
34. Werba, G. et al. Single-cell RNA sequencing reveals the effects of chemotherapy on human pancreatic adenocarcinoma and its tumor microenvironment. *Nat. Commun.* **14**, 797 (2023).
35. Hou, Z. et al. Single-cell RNA sequencing revealed subclonal heterogeneity and gene signatures of gemcitabine sensitivity in pancreatic cancer. *Front. Pharm.* **14**, 1193791 (2023).
36. Yousuf, S. et al. Spatially resolved multi-omics single-cell analyses inform mechanisms of immune dysfunction in pancreatic cancer. *Gastroenterology* **165**, 891–908.e814 (2023).
37. Longo, S. K., Guo, M. G., Ji, A. L. & Khavari, P. A. Integrating single-cell and spatial transcriptomics to elucidate intercellular tissue dynamics. *Nat. Rev. Genet.* **22**, 627–644 (2021).
38. Rao, A., Barkley, D., Franca, G. S. & Yanai, I. Exploring tissue architecture using spatial transcriptomics. *Nature* **596**, 211–220 (2021).
39. Dardare, J. et al. DDB2 represses epithelial-to-mesenchymal transition and sensitizes pancreatic ductal adenocarcinoma cells to chemotherapy. *Front. Oncol.* **12**, 1052163 (2022).
40. Krauss, L. et al. HDAC2 facilitates pancreatic cancer metastasis. *Cancer Res.* **82**, 695–707 (2022).
41. Merle, N. S., Noe, R., Halbwachs-Mecarelli, L., Fremeaux-Bacchi, V. & Roumenina, L. T. Complement System Part II: role in Immunity. *Front. Immunol.* **6**, 257 (2015).
42. Chen, K. et al. Single-cell RNA-seq reveals dynamic change in tumor microenvironment during pancreatic ductal adenocarcinoma malignant progression. *EBioMedicine* **66**, 103315 (2021).
43. Croft, W. et al. Spatial determination and prognostic impact of the fibroblast transcriptome in pancreatic ductal adenocarcinoma. *Elife* **12**, https://doi.org/10.7554/eLife.86125 (2023).
44. Ajona, D., Ortiz-Espinosa, S., Pio, R. & Lecanda, F. Complement in metastasis: a comp in the camp. *Front. Immunol.* **10**, 669 (2019).
45. Kolev, M. et al. Inside-out of complement in cancer. *Front Immunol.* **13**, 931273 (2022).
46. Pio, R., Ajona, D., Ortiz-Espinosa, S., Mantovani, A. & Lambris, J. D. Complementing the cancer-immunity cycle. *Front. Immunol.* **10**, 774 (2019).
47. West, E. E. & Kemper, C. Complosome - the intracellular complement system. *Nat. Rev. Nephrol.* **19**, 426–439 (2023).
48. Shao, F. et al. Integrating angiogenesis signature and tumor mutation burden for improved patient stratification in immune checkpoint blockade therapy for muscle-invasive bladder cancer. *Urol. Oncol.* **41**, 433.e439–433.e418 (2023).
49. Arbore, G. et al. T helper 1 immunity requires complement-driven NLRP3 inflammasome activity in CD4(+) T cells. *Science* **352**, aad1210 (2016).
50. Arbore, G. et al. Complement receptor CD46 co-stimulates optimal human CD8(+) T cell effector function via fatty acid metabolism. *Nat. Commun.* **9**, 4186 (2018).
51. van Eijck, C. W. F. et al. Enhanced antitumour immunity following neoadjuvant chemoradiotherapy mediates a favourable prognosis in women with resected pancreatic cancer. *Gut* **73**, 311–324 (2024).
52. Chouat, E. et al. Tumor budding is a prognostic factor linked to epithelial-mesenchymal transition in pancreatic ductal adenocarcinoma. Study report and literature review. *Pancreatology* **18**, 79–84 (2018).
53. Friend, C., Parajuli, P., Razzaque, M. S. & Atfi, A. Deciphering epithelial-to-mesenchymal transition in pancreatic cancer. *Adv. Cancer Res.* **159**, 37–73 (2023).
54. Kumar, S. et al. Complement-containing small extracellular vesicles from adventitial fibroblasts induce proinflammatory and metabolic reprogramming in macrophages. *JCI Insight* **6**, https://doi.org/10.1172/jci.insight.148382 (2021).
55. Keklikoglou, I. et al. Chemotherapy elicits pro-metastatic extracellular vesicles in breast cancer models. *Nat. Cell Biol.* **21**, 190–202 (2019).
56. Monteran, L. et al. Chemotherapy-induced complement signaling modulates immunosuppression and metastatic relapse in breast cancer. *Nat. Commun.* **13**, 5797 (2022).
57. Surace, L. et al. Complement is a central mediator of radiotherapy-induced tumor-specific immunity and clinical response. *Immunity* **42**, 767–777 (2015).
58. Danaher, P. et al. Advances in mixed cell deconvolution enable quantification of cell types in spatial transcriptomic data. *Nat. Commun.* **13**, 385 (2022).
59. Huang da, W., Sherman, B. T. & Lempicki, R. A. Systematic and integrative analysis of large gene lists using DAVID bioinformatics resources. *Nat. Protoc.* **4**, 44–57 (2009).

60. Sherman, B. T. et al. DAVID: a web server for functional enrichment analysis and functional annotation of gene lists (2021 update). *Nucleic Acids Res.* **50**, W216–W221 (2022).
61. Hao, Y. et al. Dictionary learning for integrative, multimodal and scalable single-cell analysis. *Nat. Biotechnol*, (2023).
62. Satija, R., Farrell, J. A., Gennert, D., Schier, A. F. & Regev, A. Spatial reconstruction of single-cell gene expression data. *Nat. Biotechnol.* **33**, 495–502 (2015).
63. Lin, H. et al. Delineation of colorectal cancer ligand-receptor interactions and their roles in the tumor microenvironment and prognosis. *J. Transl. Med.* **19**, 497 (2021).

Acknowledgements

The data collection of this study was done in the Department of Pathology and Laboratory Medicine at the University of Wisconsin-Madison (the institution X.Z. and Y.J.L. affiliated with previously). The authors thank the Translational Research Initiatives in Pathology laboratory (TRIP), supported by the UW-Madison Department of Pathology and Laboratory Medicine, UWCCC (P30 CA014520) and the Office of The Director- NIH (S10 OD023526) for use of its facilities and services. The analysis and writing of the work were completed by authors at their current institutions, i.e., NYU Grossman Long Island School of Medicine, Tulane University, and University of Washington Medical Center. The authors also thank Nancy Liu for the artistic illustration in Fig. 6C summarizing the main findings of this study.

Author contributions

X.Z., Y.Z.L., and Y.L. developed the study concept and the study design. X.Z., Y.Z.L., Y.L., and R.L. wrote the manuscript, which was then edited by all co-authors. X.Z. acquired slides and tissue blocks, collected clinical information and helped with the GeoMx experiment. X.Z. and D.L. analyzed the H&E and multiplex IHC. R.L., Y.Z.L, and X.Z. analyzed spatial transcriptomics data and conducted statistical analysis of clinicopathological information. V.G.P. provided feedback on the study design and the manuscript. C.L.Z., S.A.S., W.L., I.H., M.G., C.H., J.M., J.W., M.S., and J.A. provided feedback and edited the manuscript. All co-authors approved the final version of the manuscript before submission.

Competing interests

The authors declare no competing interests.

Additional information

Supplementary information The online version contains supplementary material available at https://doi.org/10.1038/s41698-025-00848-2.

Correspondence and requests for materials should be addressed to Xiaofei Zhang or Yao-Zhong Liu.

Reprints and permissions information is available at http://www.nature.com/reprints

Publisher's note Springer Nature remains neutral with regard to jurisdictional claims in published maps and institutional affiliations.

Open Access This article is licensed under a Creative Commons Attribution-NonCommercial-NoDerivatives 4.0 International License, which permits any non-commercial use, sharing, distribution and reproduction in any medium or format, as long as you give appropriate credit to the original author(s) and the source, provide a link to the Creative Commons licence, and indicate if you modified the licensed material. You do not have permission under this licence to share adapted material derived from this article or parts of it. The images or other third party material in this article are included in the article's Creative Commons licence, unless indicated otherwise in a credit line to the material. If material is not included in the article's Creative Commons licence and your intended use is not permitted by statutory regulation or exceeds the permitted use, you will need to obtain permission directly from the copyright holder. To view a copy of this licence, visit http://creativecommons.org/licenses/by-nc-nd/4.0/.

© The Author(s) 2025